Chemical Science

ROYAL SOCIETY OF CHEMISTRY

EDGE ARTICLE

View Article Online
View Journal | View Issue

Cite this: *Chem. Sci.*, 2022, **13**, 1009

All publication charges for this article have been paid for by the Royal Society of Chemistry

A facile and scalable synthetic method for covalent organic nanosheets: ultrasonic polycondensation and photocatalytic degradation of organic pollutants†

Shi-Xian Gan, Chao Jia, Qiao-Yan Qi and Xin Zhao *

Covalent organic framework nanosheets (COF NSs or CONs), as compared to their bulk counterparts two-dimensional (2D) covalent organic frameworks (COFs), exhibit superior performance in many aspects due to their fully accessible active sites benefiting from their ultrathin porous 2D structures. The development of a scalable synthetic methodology for CONs is crucial to further exploration of their unique properties and practical applications. Herein, we report an efficient strategy to fabricate ultrathin CONs through direct polycondensation of monomers under ultrasonic treatment and mild conditions. This method is facile and scalable, which is demonstrated by gram-scale synthesis of two ultrathin 2D CONs in several hours. Moreover, the as-prepared ultrathin CONs show excellent heterogeneous photocatalytic performance for the degradation of organic pollutants (dyes as representatives), remarkably superior to the bulk COFs prepared from the corresponding monomers under solvothermal conditions. This research provides a new roadmap for the scalable and facile synthesis of ultrathin CONs, which is of paramount importance for fully exploring the tremendous potential of this emerging type of 2D material.

Received 6th October 2021
Accepted 16th December 2021

DOI: 10.1039/d1sc05504f

rsc.li/chemical-science

Introduction

Covalent organic frameworks (COFs),[1,2] as a burgeoning class of crystalline organic polymers with permanent porosity, have garnered wide attention over the past decade due to their versatile applications in many fields ranging from catalysis,[3–6] sensing,[7–11] gas storage,[12–16] separation,[17–20] drug delivery,[21–24] nanomedicine,[25,26] to energy storage.[27–31] These applications have been enabled by the unique structural features of COFs such as ordered internal structures, well-defined nanochannels, large specific surface areas and conjugated skeletons, as well as their predesignable, tailorable, and functionalizable skeletons. COFs are usually prepared *via* solvothermal synthesis, which gives rise to insoluble polycrystalline powders (bulk COFs). While some applications, for example adsorption, are well implemented with bulk COF materials through the encapsulation of guest molecules in their extended channels, bulk COFs cannot fully exert their functions in many other application scenarios due to poor processibility and inaccessible active sites deeply buried inside the channels. In this context, COF nanosheets, also known as covalent organic nanosheets (CONs),[32] have been increasingly developing as a new type of two-dimensional (2D) material to overcome the shortcomings. Compared with bulk 2D COF materials, 2D CONs are few-layer or even single-layer materials, and thus have an extremely large aspect ratio, ultrathin thickness, and fully accessible active sites. These advantages endow them with great application potential in many aspects, such as separation,[33,34] catalysis,[35–37] energy storage,[38,39] drug delivery[40] and chemosensing.[41]

Due to the unparalleled advantages of ultrathin CONs over bulk COFs in many application scenarios, a variety of synthetic methods have been developed for them, which can be divided into two types: top-down and bottom-up.[32] The former one is based on the exfoliation of layered bulk 2D COF precursors, including sonication exfoliation,[42,43] chemical exfoliation,[44–47] self-exfoliation,[48–50] and mechanical exfoliation.[51,52] Among them, sonication exfoliation in the liquid phase is a widely used approach to delaminate layered materials. However, while it is a general method to fabricate 2D CONs, this procedure suffers from the difficulty of defining the size, thickness and shape of nanosheets. Furthermore, an inescapable problem of sonication exfoliation is the quite low yield of ultrathin 2D CONs, which becomes a bottleneck to the practical application of CONs. On the other hand, COF nanosheets can also be fabricated through a bottom-up strategy, for which condensation reactions of monomers usually occur at interfaces, including

Key Laboratory of Synthetic and Self-Assembly Chemistry for Organic Functional Molecules, Center for Excellence in Molecular Synthesis, Shanghai Institute of Organic Chemistry, University of Chinese Academy of Sciences, Chinese Academy of Sciences, 345 Lingling Road, Shanghai 200032, China. E-mail: xzhao@sioc.ac.cn

† Electronic supplementary information (ESI) available: FTIR spectra, PXRD profiles, AFM images, N_2 adsorption–desorption isotherms, BET plot, pore size distribution profiles, UV-Vis DRS spectra, UV-Vis spectra and fractional atomic coordinates. See DOI: 10.1039/d1sc05504f

gas/liquid interface,[53,54] liquid/liquid interface,[55] and solid surface,[56–58] or are assisted by an external modulator.[35] To achieve ultrathin 2D CONs *via* a "bottom-up" strategy, a low concentration of organic monomers is usually required. As a result, they are typically synthesized in very small amounts, which also significantly limits the large-scale applications of 2D CONs. To break the bottleneck problem, a facile, efficient, and scalable method is highly desired. Herein, we report a novel approach to fabricate ultrathin 2D CONs on a gram-scale in a short time. This method is direct ultrasound-mediated polycondensation of monomers under mild conditions, without the use of any matrices, templates or interfaces. The photocatalytic activity of the as-prepared CONs was investigated, which revealed their excellent performance for the degradation of organic dyes.

Results and discussion

To demonstrate this novel synthetic method, two known COF structures are selected as the research objects (Scheme 1).[59] The synthetic procedure is facile and was conducted by ultrasonically treating (100 W and 40 KHz) a mixture of the monomers (gram-scale) in organic solvents in a beaker for several hours in an ice water bath under ambient pressure (see the ESI† for details). The CONs were obtained as ultrathin nanosheets, as revealed by morphological characterization. The CON prepared from the condensation of 1,3,5-benzenetricarbaldehyde (**BTCA**) and 1,3,5-tris(4-aminophenyl)-benzene (**TAPB**) was named **P-CON**, while that from **BTCA** and 2,4,6-tris(4-aminophenyl)-1,3,5-triazine (**TAPT**) was termed **T-CON**. For comparison, their corresponding bulk 2D COFs, **P-COF** and **T-COF**, were synthesized as microcrystalline powders under solvothermal conditions by heating **BTCA** with **TAPB** or **TAPT**, respectively, in organic solvents at 120 °C for 7 days in sealed tubes.

Both the as-prepared 2D CONs (**P-CON** and **T-CON**) and the bulk 2D COFs (**P-COF** and **T-COF**) were fully characterized by various techniques. As revealed by Fourier-transform infrared (FT-IR) spectroscopy (Fig. S1 and S2†), the CONs have the same chemical compositions as those of the corresponding bulk COFs, which was evidenced by the almost same spectra recorded for the CONs and the COFs. In addition, the crystalline features of the COFs and CONs were indicated by powder X-ray diffraction (PXRD). For **P-COF**, an intense peak corresponding to the (100) facet appears at 5.66°, along with three weak peaks at 9.67°, 11.17°, and 24.85° attributed to (110), (200), and (001) facets, respectively (Fig. 1a). As to **P-CON**, the intensity of diffraction peaks was much lower, and only the (100) peak was observed at the same position of the (100) peak of **P-COF** (Fig. 1b). This result suggests that **P-CON** holds the same framework structure as that of **P-COF**, but exists as ultrathin 2D sheets. Owing to the few-layer structures, the interlayer stacking in the CONs is much weaker than that in the bulk COFs, resulting in weaker crystal plane diffraction. On the basis of the PXRD data of **P-COF**, the unit cell parameters of **P-COF** were generated through Pawley refinement to be $a = b = 18.55$ Å, $c = 3.60$ Å, $\alpha = \beta = 90°$ and $\gamma = 120°$, with $R_{wp} = 4.06\%$ and $R_p = 2.89\%$ (Fig. S3†). In the case of **T-CON** and **T-COF**, a similar phenomenon was observed (Fig. 1c and d). And the unit cell parameters were calculated to be $a = b = 18.32$ Å, $c = 3.61$ Å, $\alpha = \beta = 90°$ and $\gamma = 120°$, with $R_{wp} = 5.01\%$, $R_p = 3.55\%$, based on the experimental PXRD data of **T-COF** (Fig. S4†).

The morphology of the as-prepared CONs and bulk COFs was investigated with transmission electron microscopy (TEM) and atomic force microscopy (AFM). Different from the aggregation morphology of the bulk COFs (Fig. 2a and b), the TEM images of

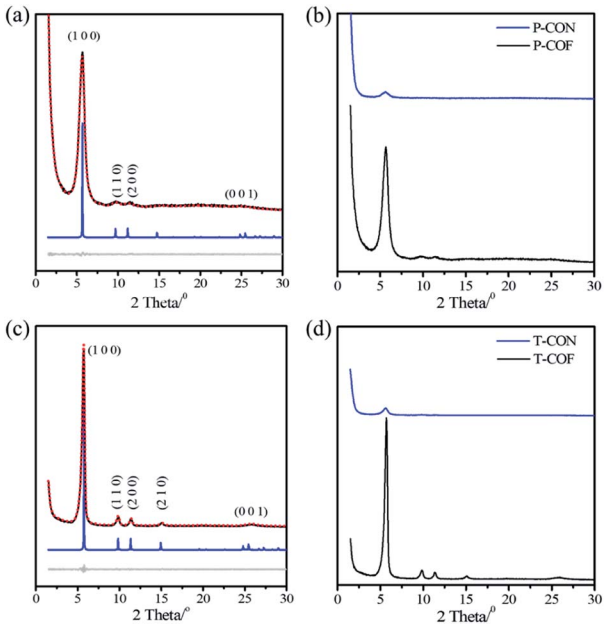

Fig. 1 (a) PXRD profiles of **P-COF**: the experimental (black), refined (red), and simulated (blue, based on eclipsed stacking) PXRD patterns, and difference plot between the experimental and refined PXRD patterns (gray). (b) Comparison between the PXRD patterns of **P-COF** and **P-CON**. (c) PXRD profiles of **T-COF**: the experimental (black), refined (red), and simulated (blue, based on eclipsed stacking) PXRD patterns, and difference plot between the experimental and refined PXRD patterns (gray). (d) Comparison between the PXRD patterns of **T-COF** and **T-CON**.

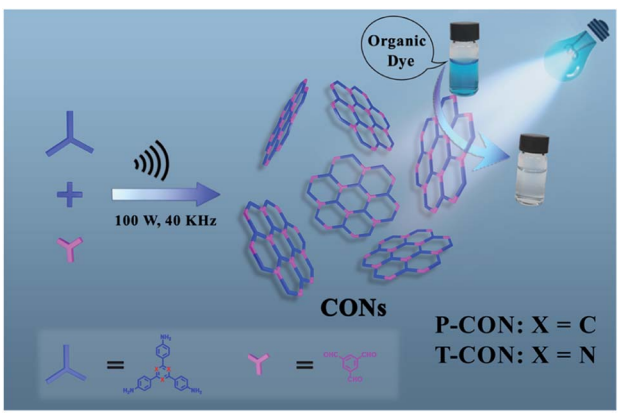

Scheme 1 Illustration for the synthesis of the ultrathin 2D CONs and their application as high-performance photocatalysts for dye degradation.

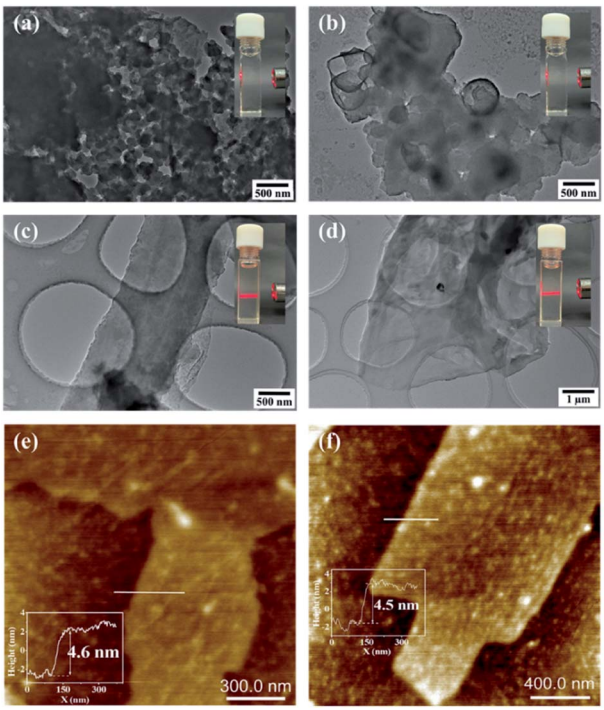

Fig. 2 TEM images of P-COF(a), T-COF (b), P-CON (c), and T-CON (d). AFM images of P-CON (e) and T-CON (f). Note: the insets in the upper right corners of (a)–(c) show the photographs recorded for testing the Tyndall effect of the dispersions of the CONs and COFs in DMSO, respectively.

the CONs show a film-like morphology with large 2D dimensions, consistent with the expected structure of nanosheets (Fig. 2c and d). Furthermore, the suspensions of **P-CON** and **T-CON** in dimethyl sulfoxide exhibit a typical Tyndall effect (the insets in Fig. 2c and d), while their corresponding bulk COFs do not (the insets in Fig. 2a and b), indicating a colloidal feature of the ultrathin 2D CON nanosheets. Impressively, the CONs exhibit a homogeneous distribution in dimethyl sulfoxide suspension without agglomeration even after two months (Fig. S5†), which is attributed to the weak interlayer stacking between the nanosheets. The thinnest thicknesses of the CONs were measured with AFM to be 4.6 nm for **P-CON** and 4.5 nm for **T-CON** (Fig. 2e and f), corresponding to about 13 stacked monolayers, while the maximum thicknesses were *ca.* 20 nm for **P-CON** and 19.6 nm for **T-CON** in a randomly selected micron range (Fig. S6†). By contrast, the bulk COFs prepared by solvothermal condensation exhibit a particle-like morphology with much larger heights (228.5 nm for **P-COF** and 565.2 nm for **T-COF** for the selected particles) (Fig. S7†). The above results clearly demonstrate the high efficiency of the ultrasonic synthesis of ultrathin CONs.

The architectural rigidity, Brunauer–Emmett–Teller (BET) surface areas, and permanent porosity of both the CONs and COFs were examined by N_2 adsorption–desorption measurements at 77 K. For **P-CON**, its BET surface area was estimated from the absorption data in the range of P/P_0 from 0.003 to 0.05, which afforded a value of 547 $m^2\ g^{-1}$. The value is much smaller than that of bulk **P-COF** (1062 $m^2\ g^{-1}$). Such a result is similar to those reported for CONs prepared by the exfoliation of bulk COFs.[45,60,61] Similarly, **T-CON** and **T-COF** also exhibit the same trend, with BET surface areas of 972 $m^2\ g^{-1}$ for **T-CON** *vs.* 1323 $m^2\ g^{-1}$ for **T-COF** (Fig. S8–S13†). Meanwhile, a smaller total pore volume of **P-CON** (0.47 $cm^3\ g^{-1}$ at $P/P_0 = 0.99$) than that of **P-COF** (0.69 $cm^3\ g^{-1}$) was found, and a similar phenomenon was also observed for **T-CON** (0.49 $cm^3\ g^{-1}$) and **T-COF** (0.65 $cm^3\ g^{-1}$). Moreover, similar to previous examples,[45] the pore size distributions of CONs are consistent with that of COFs (17.5 Å for **P-CON** *vs.* 16.7 Å for **P-COF**, and 17.8 Å for **T-CON** *vs.* 17.3 Å for **T-COF**) (Fig. S14–S17†), agreeing with their theoretical pore sizes (Fig. S18†). This result indicates that the as-prepared ultrathin 2D CONs have uniform microporous frameworks very similar to the layers in their corresponding bulk 2D COFs.

It is well known that ultrathin 2D materials have been revealed to exhibit great potential in heterogeneous photocatalysis associated with their fully accessible active sites and their large surface areas.[62] In addition to the large accessible surfaces of CONs, their porous nature also provides a strong guarantee for the adhesion of reactants, making catalytic reactions more adequate. These advantages make CONs very promising to be used as photocatalysts. Such potential was then examined for the as-prepared CONs. To this end, the photocatalytic performance of the two CONs was firstly evaluated by monitoring the degradation of methylene blue (**MB**), a typical pollutant in dyeing wastewater, under visible light irradiation. For comparison, the photocatalytic performance of their corresponding bulk 2D COFs was also investigated under analogous experimental conditions. Prior to the photocatalytic experiments, we tested the chemical stability of the COFs and CONs. Both the COFs and CONs exhibit good stability in water, as revealed by the maintenance of their crystalline structures after being immersed in water for one week (Fig. S19 and S20†).

To estimate the optical band gaps of the CONs and the COFs, their solid-state UV-Vis diffuse reflectance spectra (DRS) were recorded (Fig. S21 and S22†). These materials exhibit visible light absorption, with the maximum absorption wavelengths of 415 nm for **P-COF**, 413 nm for **P-CON**, 411 nm for **T-COF**, and 407 nm for **T-CON**. From Tauc's plots, their optical band gaps were calculated to be 2.53, 2.58, 2.47, and 2.52 eV for **P-COF**, **P-CON**, **T-COF**, and **T-CON**, respectively (Fig. S23†). The energy bands of the CONs are larger than those of their corresponding COFs, suggesting weakened conjugation of the former. It might be attributed to the lower extent of interlayer π–π interactions in the ultrathin nanosheets.[60,61] Compared to ZnO (~3.45 eV), the most commonly used photocatalyst, the as-prepared porous materials have a low optical band gap and thus are more desirable for charge transfer interactions which may lead to the generation of free radicals.[63,64] Moreover, COFs have demonstrated great potential in the field of photocatalysis,[65,66] which suggests that CONs should also be a new class of promising photocatalysts.

The photo-degradation of **MB** in water catalyzed by the CONs as well as the bulk COFs was monitored with UV-Vis spectroscopy (Fig. 3 and S24†). The results indicate that the 2D CONs show much higher photocatalytic activity than their

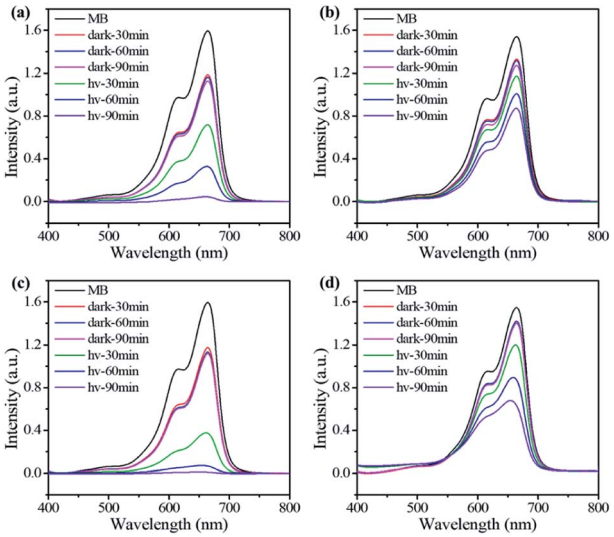

Fig. 3 UV-Vis spectra recorded for photocatalytic degradation of MB in water by P-CON (a), P-COF (b), T-CON (c), and T-COF (d) at different times.

corresponding bulk COF materials (Fig. 4a). As illustrated in Fig. 4b, the photo-degradation efficiency of **P-CON** for **MB** reaches 96.2% in 90 min with a catalyst dose of 0.5 g L^{-1}, which is more than three times that of **P-COF** (31.3%). For **T-CON**, its photo-degradation efficiency for **MB** is as high as 99.8% in 90 min with the same catalyst dose (Fig. 4c), which further proves that the as-prepared ultrathin 2D CONs have much better photocatalytic performance than the bulk 2D COFs. Moreover, as shown in Fig. 4e and f, after being reused for four cycles, **P-CON** and **T-CON** still maintain good photocatalytic activity. The slight decrease in the efficiency after each cycle is attributed to the slight loss of the CONs during sampling in the monitoring reaction and filtering process. PXRD tests after each cycle revealed that the CONs maintained their framework structures during the photocatalytic reactions, indicating their high chemical stability and good recyclability (Fig. S25†). To establish the **MB** degradation reaction kinetics, the kinetic data of the photocatalytic reaction were fitted using the Langmuir–Hinshelwood kinetics model ($\ln(C_0/C_t) = kt$, where C_0 and C_t are the concentrations of **MB** aqueous solution at $t = 0$ and t minutes of the photocatalytic reaction). As can be seen in Fig. 4d, the model indicates pseudo-first-order reaction kinetics. **T-CON** shows a high catalytic performance in the degradation of **MB** with a reaction rate constant of 6.6 × 10^{-2} min^{-1}, which is 8.25-fold higher than that of **T-COF** (8.0 × 10^{-3} min^{-1}). The same situation occurs for **P-CON** and **P-COF**, which shows that the reaction rate constant of **P-CON** (3.2 × 10^{-2} min^{-1}) is 8-fold larger than that of **P-COF** (4.0 × 10^{-3} min^{-1}). This result further confirms that the photocatalytic performance of the ultrathin 2D CONs (**P-CON** and **T-**

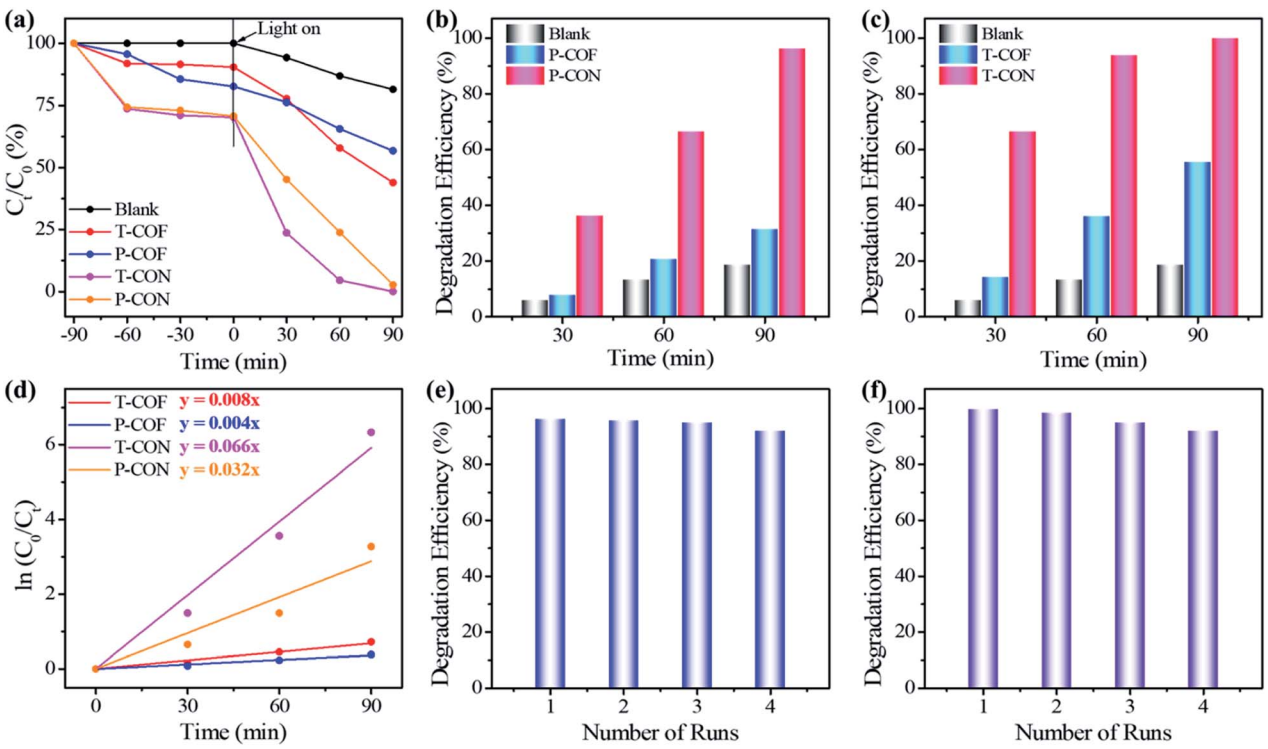

Fig. 4 Photocatalytic performance of the CONs and COFs for the degradation of MB in aqueous solutions under visible light irradiation for different times (a). Comparison of the efficiency of blank, P-COF and P-CON for photocatalytic degradation of MB in aqueous solutions for different times (b). Comparison of the efficiency of blank, T-COF and T-CON for photocatalytic degradation of MB in aqueous solutions for different times (c). Pseudo-first-order kinetic curves of photocatalytic degradation of MB in aqueous solutions (d). The cycle efficiency of P-CON (e) and T-CON (f) for photocatalytic degradation of MB in aqueous solutions.

CON) is far superior to that of the bulk 2D COFs (**P-COF** and **T-COF**).

To further evaluate the photocatalytic activity of the aforementioned CONs for the removal of organic pollutants, another organic dye, thionine acetate salt (**Th**), was also selected as the object of photo-degradation. The experimental results indicated that both **P-CON** and **T-CON** showed excellent performance to catalyze the photo-degradation of **Th**, and their efficiencies are also much higher than those of their corresponding bulk COF materials (Fig. S26 and S27†). **T-CON** showed high catalytic performance with a degradation efficiency of 96.6% in 120 min and a reaction rate constant of 2.8×10^{-2} min^{-1}, much better than **T-COF** which displayed a degradation efficiency of 65.0% and a reaction rate constant of 8.0×10^{-3} min^{-1} under the same test conditions (Fig. S28 and S30†). Notably, the degradation efficiency of **T-CON** for **Th** was up to 51.2% in 30 min, which was about 3.5 times higher than that of **T-COF** (14.5%) (Fig. S30†). In the case of **P-CON** and **P-COF**, the photocatalytic performance of **P-CON** (a degradation efficiency of 92.6% in 120 min and a reaction rate constant of 1.6×10^{-2} min^{-1}) was also much higher than that of **P-COF** (a degradation efficiency of 55.5% in 120 min and a reaction rate constant of 6.0×10^{-3} min^{-1}) (Fig. S28 and S29†). Their photocatalytic activity at the early stage of the degradation reaction was also compared, which indicated that the degradation efficiency of **P-CON** (22.0%) was 2.27-fold higher than that of **P-COF** (9.7%) in 30 min (Fig. S29†). Simultaneously, the degradation efficiency of **P-CON** (89.0%) and **T-CON** (93.2%) can be well retained after four cycles (Fig. S31 and S32†), with negligible changes of their structures, as revealed by the PXRD study (Fig. S33†). These results again suggest that the ultrathin 2D CONs exhibit superior photocatalytic performance and have a great application prospect in treating environmental pollution.

In order to investigate the photocatalytic mechanism, trapping experiments were carried out. We took the photocatalytic degradation of MB by **T-CON** as a representative to explore the mechanism of the photocatalysis. It is generally accepted that the superoxide radical ($^{\bullet}O_2^-$), photo-generated hole (h^+), and $^{\bullet}OH$ are possible reactive species in the photocatalytic degradation of organic pollutants.[67,68] To test the role of these reactive species in the photocatalysis, *p*-benzoquinone (BQ), triethanolamine (TEOA) and isopropylalcohol (IPA) were employed as scavengers for $^{\bullet}O_2^-$, h^+ and $^{\bullet}OH$, respectively. It was found that the photodegradation efficiency of **T-CON** for MB decreased after adding the three trapping reagents (Fig. S34†), indicating that $^{\bullet}O_2^-$, h^+ and $^{\bullet}OH$ were all involved in the degradation process. Moreover, when BQ was added into the reaction system, the degradation efficiency decreased remarkably (with a degradation efficiency of 49.8%), suggesting that $^{\bullet}O_2^-$ plays a crucial role in the degradation of organic pollutants.

To verify the general applicability of this method, **BTCA** was replaced by 1,3,5-triformylphloroglucinol (**Tp**) to synthesize β-keto-enamine-based CONs. The CON prepared from the condensation of **Tp** and **TAPB** was named **Tp-P-CON**, while that from **Tp** and **TAPT** was termed **Tp-T-CON**. Their framework structures were confirmed by the experimental PXRD patterns, which showed good agreement with the simulated PXRD patterns of their corresponding bulk 2D COFs (Fig. S35 and S36†). Moreover, thin layers were observed in their TEM images (Fig. S37†), suggesting the formation of nanosheet structures. These experimental results indicated that **Tp-P-CON** and **Tp-T-CON** with few layers were synthesized successfully, which demonstrated the general applicability of the method.

Conclusions

In summary, we have developed an efficient, facile, and scalable synthetic method for ultrathin 2D CONs. While in traditional top-down approaches sonication has been used as an external force to assist the delamination of layered 2D COFs to produce CONs, herein we demonstrate that CONs can be directly synthesized on a large scale through ultrasound-mediated polycondensation of monomers. Moreover, the condensation reactions are promoted by the utilization of sonication. The polymerization is completed in just a few hours under mild conditions, by which gram-scale ultrathin CONs could be obtained in one batch. The as-prepared CONs exhibit excellent photocatalytic performance in the degradation of organic pollutants in the aqueous phase, which is much higher than that of their corresponding bulk COF counterparts. The principle of this bottom-up approach is general and thus should be applicable to other COF nanosheets with different structures. With the advantages of facile operation, scalable production, and the scalability of sonication devices, this method offers facile and scalable production of ultrathin CONs, which provides a foundation for the development of practical applications of this emerging class of 2D materials.

Data availability

All the data have been included in the ESI.†

Author contributions

Conceptualization: X. Zhao and S.-X. Gan; supervision: X. Zhao; synthesis: S.-X. Gan; structural characterization: S.-X. Gan and C. Jia; photocatalytic experiments: S.-X. Gan; structural modeling: Q.-Y. Qi; manuscript writing–revising: X. Zhao and S.-X. Gan; all authors proof-read, provided comments, and approved the final version of this manuscript.

Conflicts of interest

The authors declare no competing financial interest.

Acknowledgements

We thank the National Natural Science Foundation of China (No. 21632004) and the Science and Technology Commission of Shanghai Municipality (19XD1404900) for financial support.

Notes and references

1 P. J. Waller, F. Gándara and O. M. Yaghi, *Acc. Chem. Res.*, 2015, **48**, 3053–3063.
2 K. Geng, T. He, R. Liu, S. Dalapati, K. T. Tan, Z. Li, S. Tao, Y. Gong, Q. Jiang and D. Jiang, *Chem. Soc. Rev.*, 2020, **120**, 8814–8933.
3 S.-Y. Ding, J. Gao, Q. Wang, Y. Zhang, W.-G. Song, C.-Y. Su and W. Wang, *J. Am. Chem. Soc.*, 2011, **133**, 19816–19822.
4 J. Hu, H. Mehrabi, Y.-S. Meng, M. Taylor, J.-H. Zhan, Q. Yan, M. Benamara, R. H. Coridan and H. Beyzav, *Chem. Sci.*, 2021, **12**, 7930–7936.
5 G.-B. Wang, S. Li, C.-X. Yan, F.-C. Zhu, Q.-Q. Lin, K.-H. Xie, Y. Gen and Y.-B. Dong, *J. Mater. Chem. A*, 2020, **8**, 6957–6983.
6 T. Banerjee, K. Gottschling, G. Savasci, C. Ochsenfeld and B. V. Lotsch, *ACS Energy Lett.*, 2018, **3**, 400–409.
7 G. Lin, H. Ding, D. Yuan, B. Wang and C. Wang, *J. Am. Chem. Soc.*, 2016, **138**, 3302–3305.
8 Q. Gao, X. Li, G.-H. Ning, K. Leng, B. Tian, C. Liu, W. Tang, H.-S. Xu and K. P. Loh, *Chem. Commun.*, 2018, **54**, 2349–2352.
9 L. Ascherl, E. W. Evans, J. Gorman, S. Orsborne, D. Bessinger, T. Bein, R. H. Friend and F. Auras, *J. Am. Chem. Soc.*, 2019, **141**, 15693–15699.
10 S.-Y. Ding, M. Dong, Y.-W. Wang, Y.-T. Chen, H.-Z. Wang, C.-Y. Su and W. Wang, *J. Am. Chem. Soc.*, 2016, **138**, 3031–3037.
11 D. Yan, Z. Wang, P. Cheng, Y. Chen and Z. Zhang, *Angew. Chem., Int. Ed.*, 2021, **60**, 6055–6060.
12 C. J. Doonan, D. J. Tranchemontagne, T. G. Glover, J. R. Hunt and O. M. Yaghi, *Nat. Chem.*, 2010, **2**, 235–238.
13 Y. Zeng, R. Zou and Y. Zhao, *Adv. Mater.*, 2016, **28**, 2855–2873.
14 Q. Gao, X. Li, G.-H. Ning, H.-S. Xu, C. Liu, B. Tian, W. Tang and K. P. Loh, *Chem. Mater.*, 2018, **30**, 1762–1768.
15 Y. Ding, Y. Wang, Y. Su, Z. Yang, J. Liu, X. Hua and H. Wei, *Chin. Chem. Lett.*, 2020, **31**, 193–196.
16 Y. Yang, M. Faheem, L. Wang, Q. Meng, H. Sha, N. Yang, Y. Yuan and G. Zhu, *ACS Cent. Sci.*, 2018, **4**, 748–754.
17 H. Yang, L. Yang, H. Wang, Z. Xu, Y. Zhao, Y. Luo, N. Nasir, Y. Song, H. Wu, F. Pan and Z. Jiang, *Nat. Commun.*, 2019, **10**, 2101.
18 J. Huang, X. Han, S. Yang, Y. Cao, C. Yuan, Y. Liu, J. Wang and Y. Cui, *J. Am. Chem. Soc.*, 2019, **141**, 8996–9003.
19 H. Fan, M. Peng, I. Strauss, A. Mundstock, H. Meng and J. Caro, *J. Am. Chem. Soc.*, 2020, **142**, 6872–6877.
20 Z. Jia, Z. Yan, J. Zhang, Y. Zou, Y. Qi, X. Li, Y. LI, X. Guo, C. Yang and L. Ma, *ACS Appl. Mater. Interfaces*, 2021, **13**, 1127–1134.
21 Q. Fang, J. Wang, S. Gu, R. B. Kaspar, Z. Zhuang, J. Zheng, H. Guo, S. Qiu and Y. Yan, *J. Am. Chem. Soc.*, 2015, **137**, 8352–8355.
22 V. S. Vyas, M. Vishwakarma, I. Moudrakovski, F. Haase, G. Savasci, C. Ochsenfeld, J. P. Spatz and B. V. Lotsch, *Adv. Mater.*, 2016, **28**, 8749–8754.
23 L. Bai, S. Z. F. Phua, W. Q. Lim, A. Jana, Z. Luo, H. P. Tham, L. Zhao, Q. Gao and Y. Zhao, *Chem. Commun.*, 2016, **52**, 4128–4131.
24 G. Zhang, X. Li, Q. Liao, Y. Liu, K. Xi, W. Huang and X. Jia, *Nat. Commun.*, 2018, **9**, 2785.
25 Q. Guan, L.-L. Zhou, Y.-A. Li, W.-Y. Li, S. Wang, C. Song and Y.-B. Dong, *ACS Nano*, 2019, **13**, 13304–13316.
26 Q. Guan, L.-L. Zhou, F.-H. Lv, W.-Y. Li, Y.-A. Li and Y.-B. Dong, *Angew. Chem., Int. Ed.*, 2020, **59**, 18042–18047.
27 X. Zhao, P. Pachfule and A. Thomas, *Chem. Soc. Rev.*, 2021, **50**, 6871–6913.
28 J. Li, X. Jing, Q. Li, S. Li, X. Gao, X. Feng and B. Wang, *Chem. Soc. Rev.*, 2020, **49**, 3565–3604.
29 F. Xu, H. Xu, X. Chen, D. Wu, Y. Wu, H. Liu, C. Gu, R. Fu and D. Jiang, *Angew. Chem., Int. Ed.*, 2015, **54**, 6814–6818.
30 M. Li, J. Liu, Y. Li, G. Xing, X. Yu, C. Peng and L. Chen, *CCS Chem.*, 2020, **2**, 696–706.
31 A. K. M, M. Ghosh, V. Vijayakumar, A. Halder, M. Nurhuda, S. Kumar, M. Addicoat, S. Kurungot and R. Banerjee, *Chem. Sci.*, 2019, **10**, 8889–8894.
32 D. Rodríguez-San-Miguel, C. Montoro and F. Zamora, *Chem. Soc. Rev.*, 2020, **49**, 2291–2302.
33 Y. Ying, M. Tong, S. Ning, S. K. Ravi, S. B. Peh, S. C. Tan, S. J. Pennycook and D. Zhao, *J. Am. Chem. Soc.*, 2020, **142**, 4472–4480.
34 J. Yao, C. Liu, X. Liu, J. Guo, S. Zhang, J. Zheng and S. Li, *J. Membr. Sci.*, 2020, **601**, 117864.
35 W. Liu, X. Li, C. Wang, H. Pan, W. Liu, K. Wang, Q. Zeng, R. Wang and J. Jiang, *J. Am. Chem. Soc.*, 2019, **141**, 17431–17440.
36 M. Luo, Q. Yang, W. Yang, J. Wang, F. He, K. Liu, H. Cao and H. Yan, *Small*, 2020, **16**, 2001100–2001108.
37 X. Wang, Z. Fu, L. Zheng, C. Zhao, X. Wang, S. Y. Chong, F. McBride, R. Raval, M. Bilton, L. Liu, X. Wu, L. Chen, R. S. Sprick and A. I. Cooper, *Chem. Mater.*, 2020, **32**, 9107–9114.
38 J. Sun, A. Klechikov, C. Moise, M. Prodana, M. Enachescu and A. V. Talyzin, *Angew. Chem., Int. Ed.*, 2018, **57**, 1034–1038.
39 S. Wang, Q. Wang, P. Shao, Y. Han, X. Gao, L. Ma, S. Yuan, X. Ma, J. Zhou, X. Feng and B. Wang, *J. Am. Chem. Soc.*, 2017, **139**, 4258–4261.
40 S. Mitra, H. S. Sasmal, T. Kundu, S. Kandambeth, K. Illath, D. D. Díaz and R. Banerjee, *J. Am. Chem. Soc.*, 2017, **139**, 4513–4520.
41 Y. Peng, T. Huang, Y. Zhu, B. Chen, L. Wang, Z. Lai, Z. Zhang, M. Zhao, C. Tan, N. Yang, F. Shao, Y. Han and H. Zhang, *J. Am. Chem. Soc.*, 2017, **139**, 8698–8704.
42 I. Berlanga, M. L. Ruiz-González, J. M. González-Calbet, J. L. G. Fierro, R. Mas-Ballesté and F. Zamora, *Small*, 2011, **7**, 1207–1211.
43 G. Das, B. P. Biswal, S. Kandambeth, V. Venkatesh, G. Kaur, M. Addicoat, T. Heine, S. Vermab and R. Banerjee, *Chem. Sci.*, 2015, **6**, 3931–3939.
44 X. Chen, Y. Li, L. Wang, Y. Xu, A. Nie, Q. Li, F. Wu, W. Sun, X. Zhang, R. Vajtai, P. M. Ajayan, L. Chen and Y. Wang, *Adv. Mater.*, 2019, **31**, 1901640.
45 Y. Yusran, H. Li, X. Guan, D. Li, L. Tang, M. Xue, Z. Zhuang, Y. Yan, V. Valtchev, S. Qiu and Q. Fang, *Adv. Mater.*, 2020, **32**, 1907289.

46 M. A. Khayum, S. Kandambeth, S. Mitra, S. B. Nair, A. Das, S. S. Nagane, R. Mukherjee and R. Banerjee, *Angew. Chem., Int. Ed.*, 2016, **55**, 15604–15608.
47 D. W. Burke, C. Sun, I. Castano, N. C. Flanders, A. M. Evans, E. Vitaku, D. C. McLeod, R. H. Lambeth, L. X. Chen, N. C. Gianneschi and W. R. Dichtel, *Angew. Chem., Int. Ed.*, 2020, **59**, 5165–5171.
48 S. Mitra, S. Kandambeth, B. P. Biswal, A. Khayum, C. K. Choudhury, M. Mehta, G. Kaur, S. Banerjee, A. Prabhune, S. Verma, S. Roy, U. K. Kharul and R. Banerjee, *J. Am. Chem. Soc.*, 2016, **138**, 2823–2828.
49 S. Haldar, K. Roy, S. Nandi, D. Chakraborty, D. Puthusseri, Y. Gawli, S. Ogale and R. Vaidhyanathan, *Adv. Energy Mater.*, 2018, **8**, 1702170.
50 D. N. Bunck and W. R. Dichtel, *J. Am. Chem. Soc.*, 2013, **135**, 14952–14955.
51 S. Chandra, S. Kandambeth, B. P. Biswal, B. Lukose, S. M. Kunjir, M. Chaudhary, R. Babarao, T. Heine and R. Banerjee, *J. Am. Chem. Soc.*, 2013, **135**, 17853–17861.
52 H. Liu, Q. Li, Y. Zhu, M. Zhang, R. Liu, X. Li, X. Kang, Z. Li and S. Qiao, *J. Mater. Chem. C*, 2018, **6**, 722–725.
53 W. Dai, F. Shao, J. Szczerbinski, R. McCaffrey, R. Zenobi, Y. Jin, A. D. Schlüter and W. Zhang, *Angew. Chem., Int. Ed.*, 2016, **55**, 213–217.
54 K. Liu, H. Qi, R. Dong, R. Shivhare, M. Addicoat, T. Zhang, H. Sahabudeen, T. Heine, S. Mannsfeld, U. Kaiser, Z. Zheng and X. Feng, *Nat. Chem.*, 2019, **11**, 994–1000.
55 D. Zhou, X. Tang, H. Wu, L. Tian and M. Li, *Angew. Chem., Int. Ed.*, 2019, **58**, 1376–1381.
56 Y.-P. Mo, X.-H. Liu and D. Wang, *ACS Nano*, 2017, **11**, 11694–11700.
57 T. Joshi, C. Chen, H. Li, C. S. Diercks, G. Wang, P. J. Waller, H. Li, J.-L. Bredas, O. M. Yaghi and M. F. Crommie, *Adv. Mater.*, 2019, **31**, 1805941.
58 X. Shi, D. Ma, F. Xu, Z. Zhang and Y. Wang, *Chem. Sci.*, 2020, **11**, 989–996.
59 J. Dong, Y. Wang, G. Liu, Y. Cheng and D. Zhao, *CrystEngComm*, 2017, **19**, 4899–4904.
60 J. Dong, X. Li, K. Zhang, Y. D. Yuan, Y. Wang, L. Zhai, G. Liu, D. Yuan, J. Jiang and D. Zhao, *J. Am. Chem. Soc.*, 2018, **140**, 4035–4046.
61 J. Dong, X. Li, S. B. Peh, Y. D. Yuan, Y. Wang, D. Ji, S. Peng, G. Liu, S. Ying, D. Yuan, J. Jiang, S. Ramakrishna and D. Zhao, *Chem. Mater.*, 2018, **31**, 146–160.
62 H. Zhang, *ACS Nano*, 2015, **9**, 9451–9469.
63 S. Roy, S. P. Mondal, S. K. Ray and K. Biradha, *Angew. Chem., Int. Ed.*, 2012, **51**, 12012–12015.
64 K. Preet, G. Gupta, M. Kotal, S. K. Kansal, D. B. Salunke, H. K. Sharma, S. C. Sahoo, P. V. D. Voort and S. Roy, *Cryst. Growth Des.*, 2019, **19**, 2525–2530.
65 Y. Qian, D. Li, Y. Han and H.-L. Jiang, *J. Am. Chem. Soc.*, 2020, **142**(49), 20763–22077.
66 Y.-N. Gong, W. Zhong, Y. Li, Y. Qiu, L. Zheng, J. Jiang and H.-L. Jiang, *J. Am. Chem. Soc.*, 2020, **142**(39), 16723–16731.
67 B. Wang, Z. Xie, Y. Li, Z. Yang and L. Chen, *Macromolecules*, 2018, **51**, 3443–3449.
68 Y. Yang, H. Niu, L. Xu, H. Zhang and Y. Cai, *Appl. Catal., B*, 2020, **269**, 118799.